Thermodynamic modelling of phase evolution in alkali-activated slag cements exposed to carbon dioxide

Xinyuan Ke[a,*], Susan A. Bernal[b], John L. Provis[c], Barbara Lothenbach[d]

[a] *Department of Architecture and Civil Engineering, The University of Bath, United Kingdom*
[b] *School of Civil Engineering, University of Leeds, United Kingdom*
[c] *Department of Materials Science and Engineering, The University of Sheffield, United Kingdom*
[d] *Empa, Laboratory for Concrete & Construction Chemistry, CH-8600 Dübendorf, Switzerland*

ARTICLE INFO

ABSTRACT

Carbonation of cementitious materials induced by their interaction with atmospheric CO_2 is one of the main degradation mechanisms threatening their durability. In this study, a novel thermodynamic model to predict the phase evolution of alkali-activated slags exposed to an accelerated carbonation environment is presented. This model predicts the phase assemblages of carbonated alkali-activated slag cements, as a function of CO_2 uptake under 1 v/v % CO_2 conditions, considering the bulk slag chemistry and activators used. The changes taking place during the carbonation process regarding the physicochemical properties of the main binding gel, an alkali calcium aluminosilicate hydrate (C-(N)-A-S-H), the secondary reaction products Ca−Al and Mg−Al layered double hydroxides, and amorphous aluminosilicate gels, were simulated and discussed. The predictions of the thermodynamic model are in good agreement with experimental data retrieved from the literature, demonstrating that this is a valuable tool for predicting long-term performance of alkali-activated slag cements.

1. Introduction

The carbonation of cementitious materials induced by atmospheric CO_2 is one of the main degradation mechanisms that can affect the durability of cement and concrete. In Portland cement based materials, portlandite (Ca (OH)$_2$) acts as a buffer phase to delay the decalcification of the main reaction product, a calcium silicate hydrate type gel [1]. However, portlandite is not typically formed as a reaction product in alkali-activated cement systems (especially alkali-activated slag cements), and so different carbonation mechanisms have been observed in these materials [2,3].

The majorities of investigations of carbonation in alkali-activated cements are based on experimental observations. Under natural conditions (~0.04% CO_2) the carbonation process of cements and concretes normally takes place slowly. Therefore, most studies of the carbonation of cementitious materials are conducted under accelerated conditions. Bernal et al. [2,4] compared the carbonation products formed in alkali-activated slags under natural and different acceleration conditions, and identified that 1% CO_2 and a relative humidity of 65% appears to be the most suitable accelerated test environment for alkali-activated slag cements, as under these carbonation conditions, the phase assemblages of carbonated specimens resembled those which are

observed in naturally carbonated specimens after several years of CO_2 exposure.

It is known that that accelerated carbonation conditions, particularly the concentration of CO_2, can play a key role in defining the process and products of the carbonation of the pore solution in alkali-activated cements. Bernal et al. [5] predicted using thermodynamic modelling the formation of denser sodium carbonates at CO_2 concentrations of < 1%, and sodium bicarbonates at more elevated CO_2 concentrations. These predictions were in good agreement with the experimental observations of Pouhet et al. [6], who identified formation of sodium carbonate in pore solutions of carbonated metakaolin upon natural carbonation, with the pH not falling below 10.5. Conversely, sodium bicarbonate and significant reduction of pH were observed in pore solutions exposed to 50% CO_2. These observations reveal how changes in the carbonation testing conditions can provide misleading results about the in-service performance of alkali-activated materials. This is particularly concerning as there is no standardised testing method for the evaluation of carbonation of these cements, meaning that the existing body of literature is very scattered in terms of testing conditions. In addition to this, considering the large variability in the chemistry of raw materials and activators used to produce alkali-activated cements, there is an urgent need to develop modelling tools

---

capable of predicting their carbonation behaviour, integrating the raw materials chemistry and mix design parameters, and considering the chemical reaction taking place in these materials when exposed to CO_2.

Recent developments in the available thermodynamic databases for cement-related phases [7] have enabled and improved the prediction of phase assemblages in cements based on the bulk chemistry of the binders. Myers et al. [8] proposed a new solid-solution model for sodium- and aluminium-substituted calcium silicate hydrate (C-(N)-A-S-H) type gels, commonly formed in alkali-activated cement, taking into consideration the charge balancing alkalis (mainly Na^+) within the gel structure. The application of this model for predicting phase assemblages in alkali-activated slag cement [8] showed good agreement with experimental observations. However, the feasibility of using thermodynamic models to simulate carbonation process of alkali-activated slag cements has not previously been explored.

In recent work by Shi et al. [9], a thermodynamic model was proposed for the carbonation process in the ternary Portland cement-metakaolin-limestone system. The modelling methods established in that study reflected the two-step decalcification processes that takes place in the main reaction product (C-S-H type gel): loss of Ca from the interlayer, then loss of Ca from the principal layer. The total mass of CO_2 bound within the solid cements, as predicted by the model, showed good agreement with data from thermogravimetric analysis. The pH profile of carbonated cement mortars predicted by a similar thermodynamic model also showed good consistency with the experimentally measured pH profile as a function of carbonation depth [10]. It is therefore proposed that a similar step-wise reaction path modelling approach might also be applied to alkali-activated slag cements for predicting the phase evolution during carbonation. However, it is critical to note the significant differences between the chemistry of these two types of cementitious binder systems.

The phase assemblages and the chemistry of gel binders formed in alkali-activated slag cements are predominantly controlled by the type of alkali-activator utilised [11–13], and the chemistry of the slag precursors [14–16]. Sodium-based activators are commonly used, mainly sodium hydroxide, sodium silicate (with different SiO_2/Na_2O ratios) and sodium carbonate. For simplification, the alkali-activated slag binder systems prepared using these activators will be denoted as NH-AAS, NS-AAS and NC-AAS respectively, throughout this paper. In comparison with sodium silicate activators, the initial setting and strength development are often faster when using sodium hydroxide as the activator [17], although less dense microstructures are developed at later age [12]. Beyond 28 days of age, the reaction products formed in these two binder systems are similar, except that C-(N)-A-S-H gel with lower Ca/Si ratio can be found in NS-AAS due to the higher availability of Si from the silicate activator [12]. In addition, the Mg,Al-layered double hydroxides (LDH) formed in NH-AAS often show higher crystallinity in comparison with those that form in NS-AAS [12,18]. Sodium carbonate has attracted increasing attention as the activator option with the lowest overall carbon emissions footprint and safer handling. The bulk Ca/Si ratio of the C-(N)-A-S-H gel in NC-AAS estimated from SEM-EDX analysis appeared to be slightly higher than that of NS-AAS and NH-AAS; and hemicarbonate and/or monocarbonate AFm phases are formed as Ca,Al-LDH type secondary phases in the NC-AAS system [16]. Regarding the chemistry of slag precursors, the availability of Al_2O_3 and MgO is critical in controlling the composition of the key C-(N)-A-S-H gel binder phase, and the accompanying Ca,Al-LDH and Mg,Al-LDH [14–16]. To develop a better understanding of the carbonation-induced gel structural changes in alkali-activated slag cements, the different physicochemical features of these reaction products will need to be assessed in detail.

In this study, thermodynamic models for predicting the phase evolution in alkali-activated slag binder systems during carbonation are presented. The influence of using different activators, and slag precursors with different chemical compositions, is investigated. Models describing NH-AAS, NS-ASS and NC-AAS systems are proposed.

Experimental data retrieved from the literature are used to support and validate the proposed models.

2. Methods and model description

2.1. Software and database

A thermodynamic modelling programme was used to predict the stable phases that may be expected to form as alkali-activated slag cements react with CO_2. The open source software GEM-Selektor v.3 (http://gems.web.psi.ch/GEMS3/) was utilised to perform the modelling. An extended Debye–Hückel equation was used for calculating the activity coefficients of the aqueous species, Eq. (1):

$$\log_{10} \gamma_i = \frac{-Az_i^2\sqrt{I}}{1 + Ba\sqrt{I}} + bI + \log_{10} \frac{x_{iw}}{X_w} \tag{1}$$

where γ_i is the activity coefficient, z_i is the charge of the ith aqueous species, and A ($kg^{0.5}$ $mol^{-0.5}$) and B ($kg^{0.5}$ $mol^{-0.5}$ cm^{-1}) are the temperature- and pressure-dependent electrostatic parameters. It was assumed that the aqueous phase is dominated by NaOH, so the average ion size and parameter for common short-range interactions of charged species (a and b as shown in Eq. (1)) are 3.31 Å and 0.098 kg·mol^{-1} [19]. The term x_{iw} represents the molar quantity of water, and X_w is the total molar amount of the aqueous phase. I is the total ionic strength of the aqueous solution, which was calculated using Eq. (2)

$$I = \frac{1}{2} \sum c_i \cdot z_i^2 \tag{2}$$

where c_i is the concentration of the ith ionic species and z_i is its charge.

The recently published Cemdata18 [7] was used as the main chemical thermodynamic database. The solid solution models for alkali-substituted calcium aluminate silicate hydrate gels (CNASH_ss) and for hydroxylated hydrotalcite (MgAl-OH-LDH_ss) were used, as described in detail in [8,20]. The chemical compositions of the end members of these two solid solutions are shown in Table 1. The formation of quartz, dolomite, thaumasite, and magnesite were excluded in the calculations due to their slow formation kinetics under ambient conditions [10].

2.2. Additional phases included for modelling

In addition to the Cemdata18 database, a further 15 zeolites from the MINES database (http://tdb.mines.edu/tutorials.html) were also included in the model as candidate phases. However, zeolites known to form under hydrothermal conditions (temperature > 100 °C) have been excluded from the calculation, including laumontite, leonhardite, mesolite, wairakite and yugawaralite [21]. Mordenite-(Na) and mordenite-(Ca) with bulk Si/Al = 5 have also been excluded from the calculation, as the formation of Q^4(0Al) silica species in carbonated alkali-activated slag cement has barely been observed [15,22] due to the greater tendency to form Al-connected Q^4 silica species when Al is present [23,24]. Table 2 shows the detailed thermodynamic properties of the eight zeolites included in the calculation in this study. Scolectite ($CaAl_2Si_3O_{10}·3H_2O$) was treated as the calcium end-member of the natrolite-type zeolites and was introduced into the model as Na-Ca_NAT_ss, an ideal solid solution with sodium natrolite ($Na_2Al_2Si_3O_{10}·2H_2O$). The thermodynamic properties of nine alkaline carbonate salts have also been included, as shown in Table 1.

The thermodynamic properties of carbonated hydrotalcite were estimated from the ion-exchange constant provided by Miyata [30], where a 0.42 log units higher stability for carbonate than for hydroxyl hydrotalcite was observed (Eq. (3)).
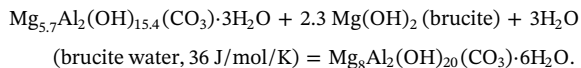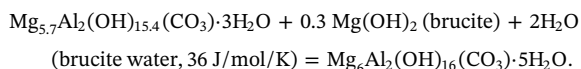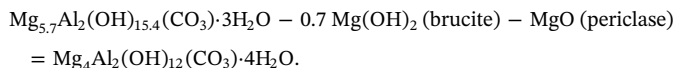
$$\log K_{ex[OH-CO_3]} = \log\left(\frac{\{Mg_{0.7}Al_{0.3}(OH)_2(OH)_{0.3}·nH_2O\}\{OH^-\}^{0.3}}{\{Mg_{0.7}Al_{0.3}(OH)_2(CO_3)_{0.15}·nH_2O\}\{CO_3^{2-}\}^{0.15}}\right)$$
$$= -0.42 \tag{3}$$

Table 1

Chemical compositions of end members in CNASH_ss solid solution and MgAl-OH-LDH_ss solid solution. These end members are consistent with the thermodynamic data entries included in the Cemdata18 database [7].

CNASH_ss

End member	Chemical formula	Bulk Ca/Si	Bulk Al/Si
With interlayer Na^+ and Ca^{2+}			
5CNA	$(CaO)_{1.25}(SiO_2)_1(Al_2O_3)_{0.125}(Na_2O)_{0.25}(H_2O)_{1.375}$	1.25	0.25
With only interlayer Ca^{2+}			
5CA	$(CaO)_{1.25}(SiO_2)_1(Al_2O_3)_{0.125}(H_2O)_{1.625}$	1.25	0.25
T2C	$(CaO)_{1.5}(SiO_2)_1(H_2O)_{2.5}$	1.50	0
T5C	$(CaO)_{1.25}(SiO_2)_{1.25}(H_2O)_{2.5}$	1.00	0
With only interlayer Na^+			
INFCN	$(CaO)_1(SiO_2)_{1.5}(Na_2O)_{0.3125}(H_2O)_{1.1875}$	0.67	0
INFCNA	$(CaO)_1(SiO_2)_{1.1875}(Al_2O_3)_{0.15625}(Na_2O)_{0.34375}(H_2O)_{1.3125}$	0.84	0.26
Without interlayer Na^+ and Ca^{2+}			
INFCA	$(CaO)_1(SiO_2)_{1.1875}(Al_2O_3)_{0.15625}(H_2O)_{1.65625}$	0.84	0.26
TobH	$(CaO)_1(SiO_2)_{1.5}(H_2O)_{2.5}$	0.67	0

MgAl-OH-LDH_ss

End member	Chemical formula	Bulk Mg/Al
M4A-OH-LDH	$Mg_4Al_2(OH)_{14}\cdot3H_2O$	2.0
M6A-OH-LDH	$Mg_6Al_2(OH)_{18}\cdot3H_2O$	3.0
M8A-OH-LDH	$Mg_8Al_2(OH)_{22}\cdot3H_2O$	4.0

If normalised to one carbonate per formula unit, the difference is 2.8 log units per CO_3-hydrotalcite. The same difference was applied to all Mg/Al ratios. The stabilisation of the carbonate-containing hydrotalcite relative to hydrotalcite-group phases containing a single anion such as OH^- has also been suggested by Allada et al. [31] based on enthalpy measurements. The entropy values, S, were estimated from the entropy value of 658 J/mol/K for $Mg_{5.7}Al_2(OH)_{15.4}(CO_3)\cdot3H_2O$ [32] assuming $\Delta S_r = 0$ [33] for the reactions as indicated in the footnotes to Table 2:

$$Mg_{5.7}Al_2(OH)_{15.4}(CO_3)\cdot3H_2O - 0.7\,Mg(OH)_2\,(brucite) - MgO\,(periclase)$$
$$= Mg_4Al_2(OH)_{12}(CO_3)\cdot4H_2O.$$

$$Mg_{5.7}Al_2(OH)_{15.4}(CO_3)\cdot3H_2O + 0.3\,Mg(OH)_2\,(brucite) + 2H_2O$$
$$(brucite\,water,\,36\,J/mol/K) = Mg_6Al_2(OH)_{16}(CO_3)\cdot5H_2O.$$

$$Mg_{5.7}Al_2(OH)_{15.4}(CO_3)\cdot3H_2O + 2.3\,Mg(OH)_2\,(brucite) + 3H_2O$$
$$(brucite\,water,\,36\,J/mol/K) = Mg_8Al_2(OH)_{20}(CO_3)\cdot6H_2O.$$

2.3. Model description

2.3.1. Input parameters

The chemical composition of ground granulated blast furnace slag (GGBFS) varies from source to source. Fig. 1 shows a summary of the main chemical constituents of GGBFS from 46 different slags reported in 31 different sources (details included in the supporting information, Table S-1). The total SO_3 content as reported in literature has been converted to equivalent H_2S to reflect the redox state of sulfur in slags.

As a baseline in this study, the composition of a conventional European slag was adopted to represent the precursor used in synthesis of the alkali-activated cement: 42.3 wt% CaO, 32.2 wt% SiO_2, 13.3 wt% Al_2O_3, 5.2 wt% MgO. An SO_3 content of 2.5 wt% has been included in the form of equivalent H_2S (1.06 wt%) in all simulations unless otherwise specified.

Equivalent activator doses between 3 and 8 wt% Na_2O (defined relative to the mass of slag; i.e. 3–8 g Na_2O per 100 g slag) have commonly been used for sodium hydroxide, silicate and carbonate

activators [18,22,34–36], and desirable early age strength development has been observed at ~4 wt% Na_2O in several cases [4,18,22]. Therefore, in this study, an activator dose of 4 wt% Na_2O was selected as a baseline case, with a water to binder (total mass of slag and the solid activator) ratio of 0.40. A 70% degree of reaction of the slag has been applied in the model, to represent approximately 28 days of curing [22,37,38]. Since the reaction kinetics of slag beyond 28 days is much slower (e.g. about 5% further reaction between 28 days and 180 days [11,16,37]) than the carbonation process under accelerated conditions (e.g. fully carbonation under 1 vol% CO_2 after 7–14 days [5,32]). Therefore, it is assumed in this study that this remains constant during the accelerated carbonation processes that are simulated here, without any significant additional hydration or weathering of slag particles being induced. The initial gas phase included as input was 8×10^{-3} g dry air (containing 21 vol% O_2) for the mix design of every 100 g of anhydrous slag (70 g reacted). This value was calculated using an estimated total sample porosity of 10% [39].

The influences of slag chemistry on the carbonation process, i.e. the influence of changing Al_2O_3 and MgO contents, have been modelled for both NS-AAS system and NC-AAS system. For this part of the study, the CaO, SiO_2 and H_2S contents of the slags were held constant, while bulk Al_2O_3 contents from 7.7 to 17.7 wt%, and correspondingly MgO contents from 11.3 to 1.3 wt% (to give a constant sum of these oxides).

2.3.1. Modelling accelerated carbonation

Stepwise CO_2 addition was used to mimic accelerated carbonation conditions, where at each step, 0.3 g of pure CO_2 gas (density 1.98 kg/m³) was added along with 18.6 g of air (density 1.22 kg/m³), equivalent to 1 vol% CO_2 throughout the carbonation stages (See Fig. S-1, supporting information). The oxygen present in the air was intended to test for the simultaneous oxidation and carbonation processes expected to occur in alkali-activated slag cements during exposure. This carbonation step size was chosen based on a prior step size sensitivity test, where CO_2 increments of 0.1 g, 0.3 g or 1 g per step were compared. Differences in phase evolution between these different step sizes were only observed within the initial 1 g of CO_2 reacted with the binder (per100 g of anhydrous slag), and so the choice of 0.3 g CO_2 per step was deemed sufficient to accurately reflect the phase evolution overall (see Figs. S-2 and S-3, Supporting information).

Table 2
Thermodynamic properties of mineral phases included for modelling in addition to the Cemdata18 database.

	$\Delta G°_f{}^a$ (kJmol^{-1})	$\Delta H°_f{}^b$ (kJmol^{-1})	$S°^c$ (Jmol^{-1} K^{-1})	Ref
Thomsonite (Si/Al = 1) $Ca_2NaAl_5Si_5O_{20}\cdot 6H_2O$	−11,453.9	−12,367.6	756.6	[25]
Scolecite (Si/Al = 1.5)^e $CaAl_2Si_3O_{10}\cdot 3H_2O$	−5598.1	−6048.8	367.4	[26]
Analcime (Si/Al = 2) $Na_{0.96}Al_{0.96}Si_{2.04}O_6\cdot 1.02H_2O$	−3082.9	−3301.8	233.6	[25]
Chabazite-(Na) (Si/Al = 2) $Na_2Al_2Si_4O_{12}\cdot 6H_2O$	−7113.5	−7782.4	619.4	[25]
Chabazite-(Ca) (Si/Al = 2) $CaAl_2Si_4O_{12}\cdot 6H_2O$	−7154.7	−7816.0	584.1	[25]
Heulandite-(Na) (Si/Al = 3.5) $Na_2Al_2Si_7O_{18}\cdot 5H_2O$	755.2	−10.2	736.2	[25]
Heulandite-(Ca) (Si/Al = 3.5) $CaAl_2Si_7O_{18}\cdot 6H_2O$	−9724.0	−10,541.3	732.5	[25]
Stilbite-(Ca) (Si/Al = 3.5) $CaAl_2Si_7O_{18}\cdot 7H_2O$	−9962.2	−10,828.6	805.3	[25]
Dawsonite $NaAlCO_3(OH)_2$	−1786.0	−1964.0	131.8	[27]
Natron $Na_2CO_3\cdot 10H_2O$	−3431.5	−4082.0	564.7	[28]
Thermonatrite $Na_2CO_3\cdot H_2O$	−1288.7	−1432.0	168.2	[28]
Gaylussite $Na_2Ca(CO_3)_2\cdot 5H_2O$	−3372.0	−3834.0	387.0	[29]
Artinite $Mg_2(CO_3)(OH)_2\cdot 3H_2O$	−2568.3	−2920.6	232.7	[28]
Huntite $CaMg_3(CO_3)_4$	−4203.5	−4529.6	299.5	[28]
Hydromagnesite (I) $Mg_4(CO_3)_3(OH)_2\cdot 3H_2O$	−4603.3	−5114.7	391.2	[28]
Hydromagnesite (II) $Mg_5(CO_3)_4(OH)_2\cdot 4H_2O$	−5864.2	−6514.9	503.7	[28]
Nesquehonite $MgCO_3\cdot 3H_2O$	−1723.7	−1977.3	195.6	[28]
CO_3_HT, Mg/Al = 2 $Mg_4Al_2(OH)_{12}(CO_3)\cdot 4H_2O^d$	−6825.1	−7678.1	587.8	This study
CO_3_HT, Mg/Al = 3 $Mg_6Al_2(OH)_{16}(CO_3)\cdot 5H_2O^d$	−8726.7	−9820.6	750.3	This study
CO_3_HT, Mg/Al = 4 $Mg_8Al_2(OH)_{20}(CO_3)\cdot 6H_2O^d$	−10,628.4	−11,963.1	912.7	This study

[a] Standard molar Gibbs energy of formation.
[b] Molar enthalpy of formation.
[c] Absolute molar entropy.
[d] $Mg_4Al_2(OH)_{12}(CO_3)\cdot 4H_2O = 4\ Mg^{2+} + 2AlO_2{}^- + 4OH^- + CO_3{}^{2-} + 8H_2O$; log K_{s0} = 52.5; $Mg_6Al_2(OH)_{16}(CO_3)\cdot 5H_2O = 6\ Mg^{2+} + 2AlO_2{}^- + 8OH^- + CO_3{}^{2-} + 9H_2O$; log K_{s0} = −74.82; $Mg_8Al_2(OH)_{20}(CO_3)\cdot 6H_2O = 8\ Mg^{2+} + 2AlO_2{}^- + 12OH^- + CO_3{}^{2-} + 10H_2O$; log K_{s0} = −97.14.
[e] Together with sodium natrolite ($Na_2Al_2Si_3O_{10}\cdot 2H_2O$), was introduced in the model as the Na-Ca_NAT_ss ideal solid solution.

3. Results and analysis

3.1. The influence of activator types

In this section, the predictions of phase evolution under step-wise carbonation, of alkali-activated slags prepared using different alkali activators, are compared. Fig. 2 to Fig. 4 show the phase assemblages and the change of pH in the aqueous phase during step-wise carbonation of slag activated by sodium hydroxide and by sodium silicate, corresponding to SiO$_2$/Na$_2$O molar ratios of 0 (Fig. 2), 1 (Fig. 3) and 2 (Fig. 4).

At zero CO$_2$ addition to the system, an alkali-substituted calcium aluminosilicate hydrate (C-(N)-A-S-H) type gel is predicted as the main reaction product, while strätlingite and hydroxylated hydrotalcite are predicted as the main secondary reaction products. A small amount of C$_3$AH$_6$ (katoite) was also predicted to form in the NH-AAS system (Fig. 2), and a small amount of natrolite (representing the amorphous alkali aluminosilicate gel observed in these cements [37,40]) for the NS-AAS system with SiO$_2$/Na$_2$O ratio of 1 and 2 (Figs. 3 and 4). The phase assemblages predicted for non-carbonated pastes are in accordance with observations from experimental characterisation of

alkali-activated slag activated by sodium hydroxide [12,41], and sodium silicate [15,42].

With increased addition of CO$_2$ and air into these systems, similar phase evolution is predicted for sodium hydroxide- and sodium silicate-activated slag cements, independent of the activator modulus (SiO$_2$/Na$_2$O ratio) used. The mass of C-(N)-A-S-H gel, C$_3$AH$_6$ and strätlingite decreased in the early stages of carbonation. Monosulfate, hemicarbonate and monocarbonate were predicted as intermediate carbonation products. After the decomposition of monosulfate, ettringite was predicted to be the main sulfate-bearing phase (with sulfate formed by oxidation of sulfide), which then further carbonated to form gypsum. Calcite was predicted as a carbonation product when monocarbonate started to decompose, and increased monotonically in mass until the full exhaustion of C-(N)-A-S-H gels. In the initial stage of carbonation, the hydroxylated hydrotalcite (MgAl-OH-LDH_ss) was transformed to carbonated hydrotalcite (MgAl-CO-LDH_ss), which converted to magnesium silicate hydrate (M-S-H) gel in the later carbonation stages. With the continuous addition of CO$_2$ after the exhaustion of C-(N)-A-S-H gels, the M-S-H gel decomposed to huntite in the presence of calcite. Different types of zeolites have been predicted to form during the carbonation process, with varying bulk Si/Al ratios and different amounts
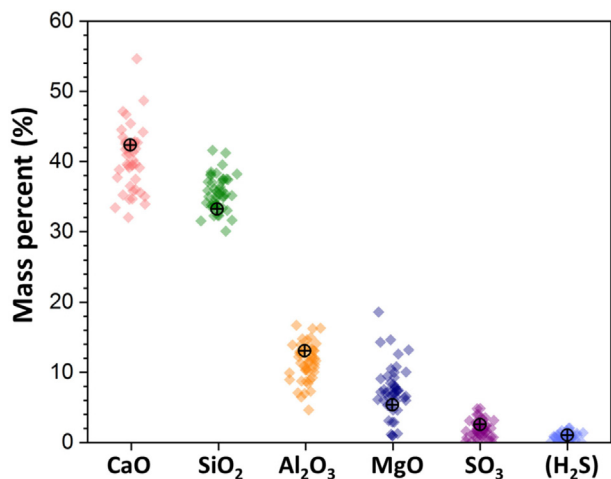
Fig. 1. Oxide compositions of 46 different ground granulated blast furnace slags (GGBFS) summarised from X-ray fluorescence results reported 31 studies. The cross-circle symbols indicate the slag composition used for the baseline case in this study.

of Na^+ and Ca^{2+} as extra-framework charge balancing cations. The bulk mass of total zeolites increased as carbonation proceeded. Note that although modelling predicts the formation of zeolites, their formation is often kinetically limited. Instead, the formation of ill-defined and rather disordered tetrahedral-coordinated aluminosilicates is more likely to occur on shorter timeframes.

The phase assemblages predicted in sodium carbonate activated slag binders before and after carbonation (Fig. 5) are very different from the systems discussed above. Prior to carbonation, C-(N)-A-S-H gel was predicted as the main reaction product in NC-AAS, together with monocarbonate and carbonated hydrotalcite. Small fraction of calcite and amorphous aluminosilicate gels have also been predicted. According to the experimental observations from samples prepared using slags of similar chemical composition to those used in the calculations here, hemicarbonate and gaylussite were identified as transient secondary phases up to 28 days, and gradually decomposed before 90 days [16]. The formation of gaylussite as a transient phase also temporarily

bound a significant amount of the CO_3^{2-} ions introduced by the activator, which can explain the preferred formation of hemicarbonate instead of monocarbonate at early age. This suggests that under experimental condition, the hydrotalcite formed in NC-AAS at early age might also be only partially carbonated, despite the high concentration of carbonate ions provided by the activators. Upon carbonation, carbonated ettringite started to form, accommodating the sulfate species. Meanwhile, monocarbonate gradually decomposed and calcite increased until the complete exhaustion of C-(N)-A-S-H gels. The carbonated hydrotalcite decomposed at a later carbonation stage, with M-S-H gels formed as the transitional magnesium-bearing phase and huntite predicted as the final magnesium-bearing phase.

Table 3 summarises the carbonation products formed in alkali-activated slag cements prepared using different activators, as observed from experimental characterisations. The main carbonation products predicted from the thermodynamic model are in good agreement with the main carbonation reaction products reported in the literature for these cements, mainly calcite and carbonated hydrotalcite. Apart from calcite, the other $CaCO_3$ polymorphs aragonite and vaterite are also commonly identified experimentally in carbonated alkali-activated cements. The standard Gibbs energies of formation of both aragonite (-1128.3 kJ/mol) and vaterite (-1125.5 kJ/mol) are slightly higher than that of calcite (-1129.2 kJ/mol) [28], therefore thermodynamic modelling will always predict calcite. However, formation of vaterite and aragonite can be kinetically preferred at early stages of precipitation as the ion activity product of calcium and carbonate decreases from the oversaturated initial conditions [43]. Vaterite has also been identified as a transitional carbonate phase before the crystal structure of calcite can be reached [44]. These metastable phases will not be predicted by a thermodynamic model as is presented here, so their observation in experiments indicates some degree of kinetic rather than thermodynamic control of reaction products in the short term.

Hydrous sodium carbonates, such as natron, trona, and thermonatrite, and carbonate double salts, such as gaylussite, have also been identified experimentally in carbonated alkali-activated cements but not predicted in this study. The identification of these phases was mostly based on single reflection peaks from X-ray diffraction analysis, suggesting that there might be only a small fraction of such phases formed in the carbonated binder systems evaluated. The formation of

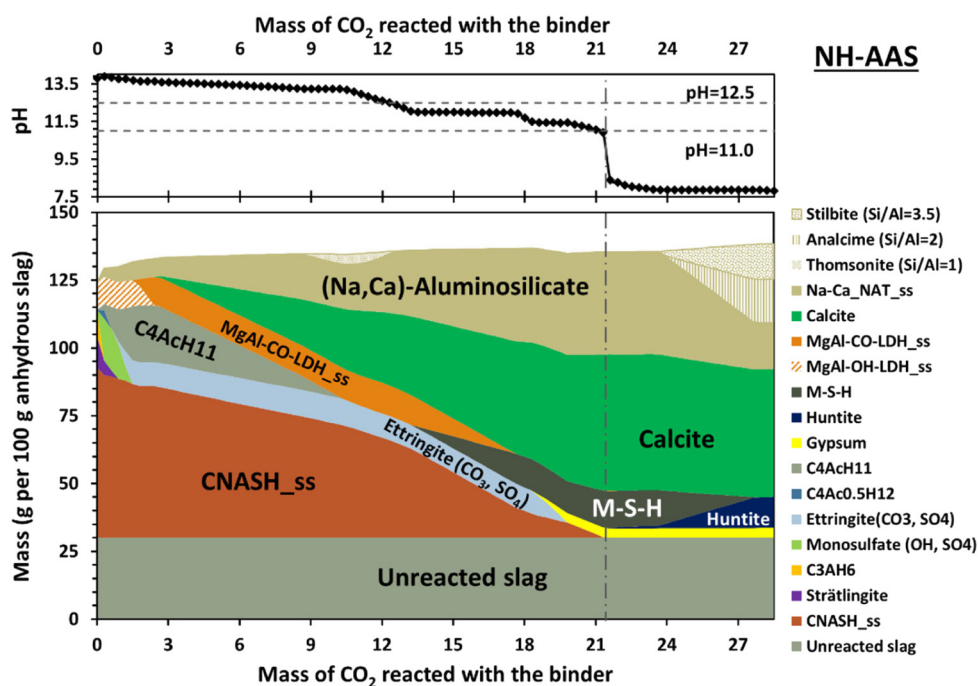**Fig. 2.** Phase assemblage of NaOH-activated slag paste (4% Na_2O, degree of slag reaction 70%) predicted under step-wise accelerated carbonation (1% CO_2), and the corresponding pH in the aqueous phase (pore solution). The horizontal dashed lines represent pH values of 12.5 and 11.0 respectively, and the vertical dash-dot line indicates the predicted phase assemblage and the pH at the exhaustion of CNASH_ss.

Fig. 3. Phase assemblage of Na$_2$O·SiO$_2$-activated slag paste (4% Na$_2$O, Na$_2$O/SiO$_2$ molar ratio of 1, degree of slag reaction 70%) predicted under step-wise accelerated carbonation (1% CO$_2$), and the corresponding pH in the aqueous phase (pore solution). The horizontal dashed lines represent pH values of 12.5 and 10.3 respectively, and the vertical dash-dot line indicates the predicted phase assemblage and the pH at the exhaustion of CNASH_ss.
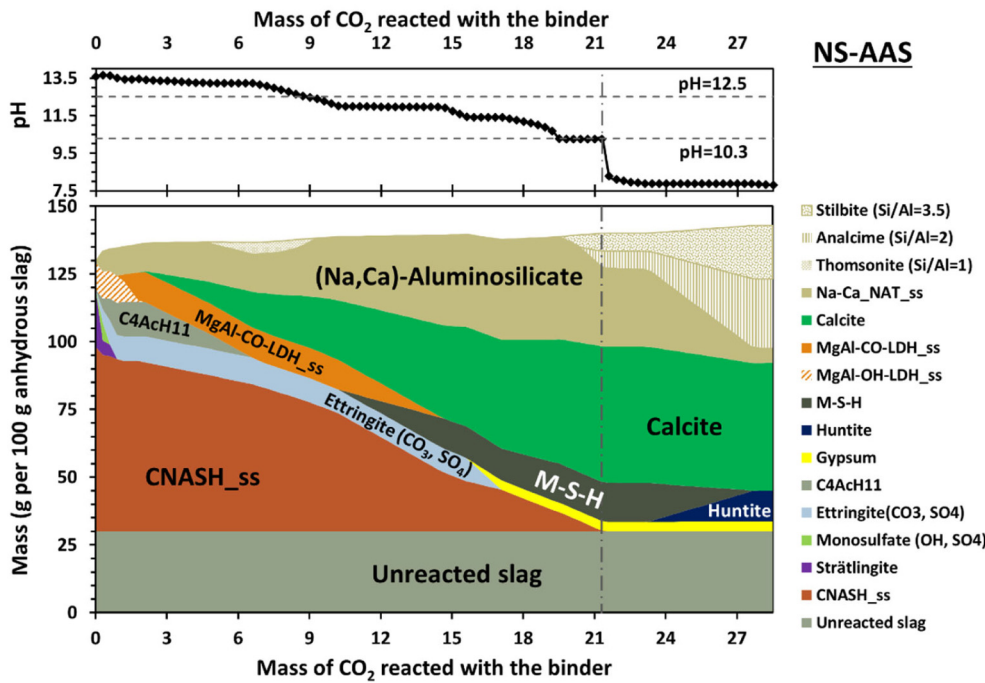
different hydrated forms of sodium carbonate under experimental conditions is due to the details of the crystallisation of sodium and carbonate ion species from the carbonated pore solution. This is influenced by the external relative humidity, and thus the drying process before analysis. As for carbonate double salts, gaylussite has been identified in non-carbonated NC-AAS pastes at early age (< 28 days of curing) as a transient phase which normally decomposes beyond 28 days of curing [16]. This suggests that the formation of gaylussite might also be kinetically favoured. Instead, huntite has been experimentally identified and thermodynamically predicted in carbonated sodium silicate-activated slag cement as the final stable magnesium-bearing phase. Huntite is preferred to form in the presence of calcite when the availability of Mg^{2+} in the system increases [29]. Although

huntite has also been predicted in the carbonated sodium hydroxide-activated and sodium carbonate-activated slag cements as the final magnesium-bearing phase, the experimental identification of this phase from the carbonated samples in these systems has not yet been reported.

3.1.1. Carbonation of C-N-A-S-H

Changes in the chemical compositions of C(N)ASH_ss (i.e. relative proportions of the different end members) predicted to occur during the carbonation process are discussed in this section (Fig. 6 to Fig. 8), including changes in the interlayer charge-balancing cations and bulk Ca/Si and Al/Si elemental ratios. Sodium hydroxide, sodium silicate (SiO$_2$/Na$_2$O = 1) and sodium carbonate-activated slag cements have been
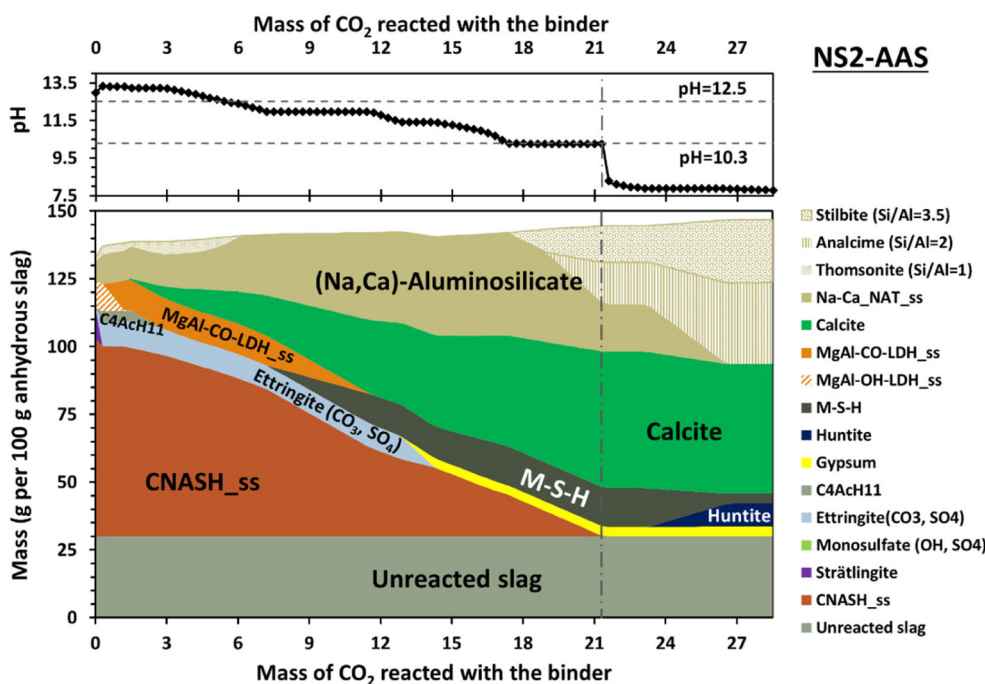
Fig. 4. Phase assemblage of Na$_2$O·2SiO$_2$-activated slag paste (4% Na$_2$O, Na$_2$O/SiO$_2$ molar ratio of 2, degree of slag reaction 70%) predicted under step-wise accelerated carbonation (1% CO$_2$), and the corresponding pH in the aqueous phase (pore solution). The horizontal dashed lines represent pH values of 12.5 and 10.3 respectively, and the vertical dash-dot line indicates the predicted phase assemblage and the pH at the exhaustion of CNASH_ss.
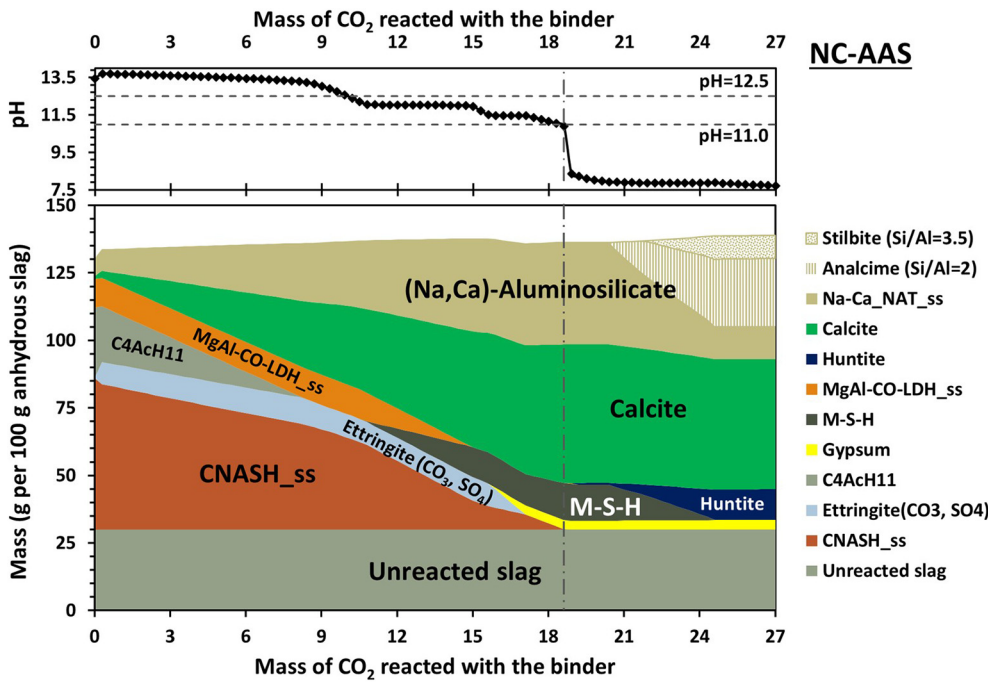
Fig. 5. Phase assemblage of Na_2CO_3-activated slag paste (4% Na_2O, degree of slag reaction 70%) predicted under step-wise accelerated carbonation (1% CO_2), and the corresponding pH in the aqueous phase (pore solution). The horizontal dashed lines represent pH values of 12.5 and 11.0 respectively, and the vertical dash-dot line indicates the predicted phase assemblage and the pH at the exhaustion of CNASH_ss.

Table 3

Summary of carbonation reaction products observed from experimental studies for alkali-activated slag paste/mortar/concrete prepared with different activators and exposed to accelerated carbonation.

| Activator type	Amount[a]	Mineral phases (carbonation products)	Ref.	Predicted by GEMS modelling
NaOH	M	Calcite	[18,36,45,46]	Y
	S	Aragonite	[45]	N
	M	Vaterite	[18,36,45,46]	N
	M	Carbonated hydrotalcite	[18,36,45,46]	Y
	S	Sodium carbonate hydrates (e.g. natron, thermonatrite)	[45]	N
	M	(Na,Ca)-aluminosilicate gel	[22]	Y
$Na_2O \cdot nSiO_2$	M	Calcite	[4,5,15,18,34,45]	Y
	M	Aragonite	[4,5,15,45]	N
	M	Vaterite	[4,5,15,18,45]	N
	M	Carbonated hydrotalcite	[18]	Y
	S	Sodium carbonate hydrates (e.g. natron, thermonatrite)	[4,5,15,34,45]	N
	S	Huntite	[4,15]	Y
	S	Carbonate double salts (e.g. gaylussite)	[4,5,15]	N
	M	(Na,Ca)-aluminosilicate gel	[4,22]	Y
Na_2CO_3	M	Calcite	[3,47]	Y
	M	Vaterite	[3,47]	N
	M[b]	Monocarbonate	[3]	Y
	M	Carbonated hydrotalcite	[3,47]	Y
	M[b]	Gaylussite	[47]	N
	M	(Na,Ca)-aluminosilicate gel	[3]	Y

[a] M: major product; S: single peak identification/only slight amount; N: not yet observed.
[b] Identified as transient carbonation products.

compared, based on the corresponding total phase evolution results shown in Figs. 2, 3 and 5 respectively. The mean chain length (MCL) of the predicted C-(N)-A-S-H gel (assuming a non-crosslinked gel structure) during the carbonation processs was calculated via Eq. (3) as proposed by Myers et al. [8], where χ_k is the molar fraction of the kth CNASH_ss end member, and ν_k is the fraction of bridging site vacancies per dreierketten unit ($\nu_{T2C} = 1$; ν_{5CA}, ν_{5CNA}, and $\nu_{T5C} = 0.5$; ν_{INFCA}, ν_{INFCNA}, ν_{INFCN}, and $\nu_{TobH} = 0$).

$$MCL = \frac{3}{\sum_k (\chi_k \nu_k)} - 1 \qquad (3)$$

As shown in Figs. 6 to 8, the changes in the main binder C-(N)-A-S-H gel for NH-AAS, NS-AAS and NC-AAS can be summarised as a three-stage decalcification process:

Stage (I) Loss of interlayer charge-balancing Na^+, while the bulk Ca/Si and Al/Si ratio as well as the MCL remain relatively unchanged. The C-(N)-A-S-H type gel containing both Na^+ and Ca^{2+} as interlayer cations decomposes first. The predicted pore solution pH declines slowly during this initial carbonation stage and remained above pH 13.2.

Stage (II) Loss of interlayer charge-balancing Ca^{2+} while the bulk Ca/Si ratio starts to decline. The tetrahedral Al in the C-(N)-A-S-H type gel is also lowered. The mass of C-A-S-H gel with no charge-balancing Na^+ and Ca^{2+} reaches the highest amount at the end of this stage while the calculated MCL increases. The predicted pore solution pH drops significantly from 13.2 to 12.0.

Stage (III) Significant loss of structural Ca^{2+} and the C-(N)-A-S-H type
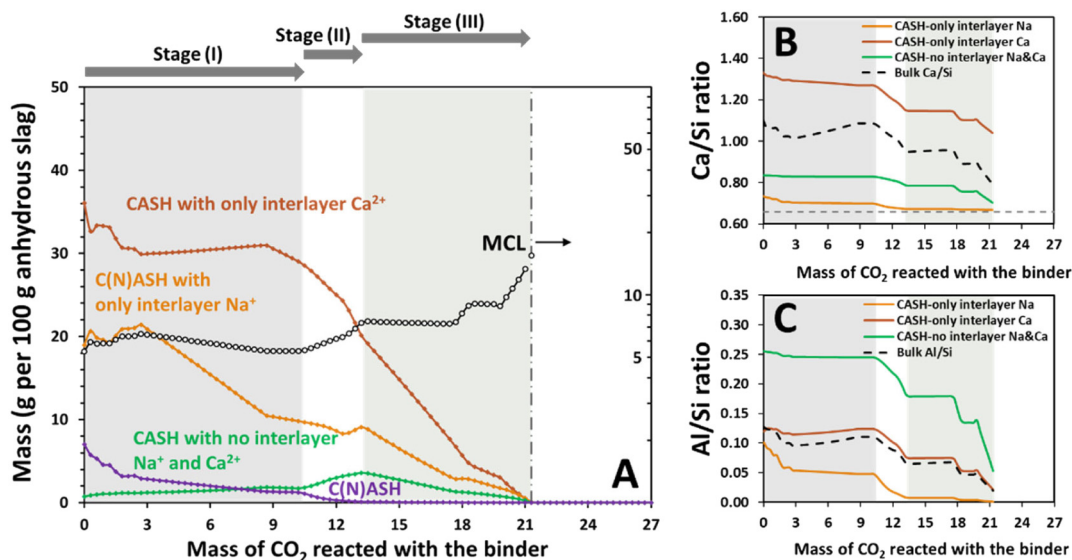
Fig. 6. (A) Mass change of different CNASH_ss end members and mean chain length (MCL) of the CNASH_ss predicted in NaOH-activated slag paste (4% Na₂O, degree of slag reaction 70%) predicted under step-wise accelerated carbonation (1% CO₂). The grouping of CNASH_ss end members are explained in Table 1. (B) Changes in the Ca/Si ratio in bulk CNASH_SS and individual C-A-S-H gels with different interlayer species. (C) Changes in the Al/Si ratio in bulk CNASH_SS and individual C-A-S-H gels with different interlayer species.

gel with both Ca^{2+} and Na^+ interlayer cations decompose. The bulk Ca/Si and Al/Si ratio remains constant until the full destabilisation of carbonated hydrotalcite (to M-S-H), and then continuous to decline. The MCL increases as the Ca/Si and Al/Si ratio decreases. The predicted pore solution pH remains at 12.0 during the decomposition of carbonated hydrotalcite, and then declines to above 10.3 until full exhaustion of the C-(N)-A-S-H type gel.

Although there is a lack of experimental data available in the literature regarding the decalcification process of C-(N)-A-S-H gel, the predictions from this study show good consistency with the experimental characterisation of C-(A)-S-H gel, where a two-step decalcification process (first the loss of interlayer Ca^{2+}, and then the loss of

structural Ca^{2+}) was observed [48]. The interlayer charge balancing Na^+ in the CNASH_ss model allows the model to reflect the high alkali content in alkali-activated cements [8], and it is reasonable to assume that the ionic bonding of the monovalent Na^+ in the interlayer would be less stable than that of the divalent Ca^{2+} charge balancing site when the aqueous pH drops. The change of Ca/Si ratio in the grouped C-(N)-A-S-H end members as carbonation proceeds (Figs. 6B, Fig. 7B and Fig. 8B) matches the trend observed for C-S-H gels with different initial bulk Ca/Si ratios [48].

The experimental results available in the literature regarding changes in the main gel binder within AAS systems were mostly based on coupled analysis of solid-state ²⁹Si MAS NMR and ²⁷Al MAS NMR. Most existing studies on the NH-AAS and NS-AAS systems give only gel structure changes after exposure to either accelerated carbonation and/

Fig. 7. (A) Mass change of different CNASH_ss end members and mean chain length (MCL) of the CNASH_ss predicted in Na₂SiO₂-activated slag paste (4% Na₂O, degree of slag reaction 70%) predicted under step-wise accelerated carbonation (1% CO₂). The grouping of CNASH_ss end members are explained in Table 1. (B) Changes in the Ca/Si ratio in bulk CNASH_SS and individual C-A-S-H gels with different interlayer species. (C) Changes in the Al/Si ratio in bulk CNASH_SS and individual C-A-S-H gels with different interlayer species.
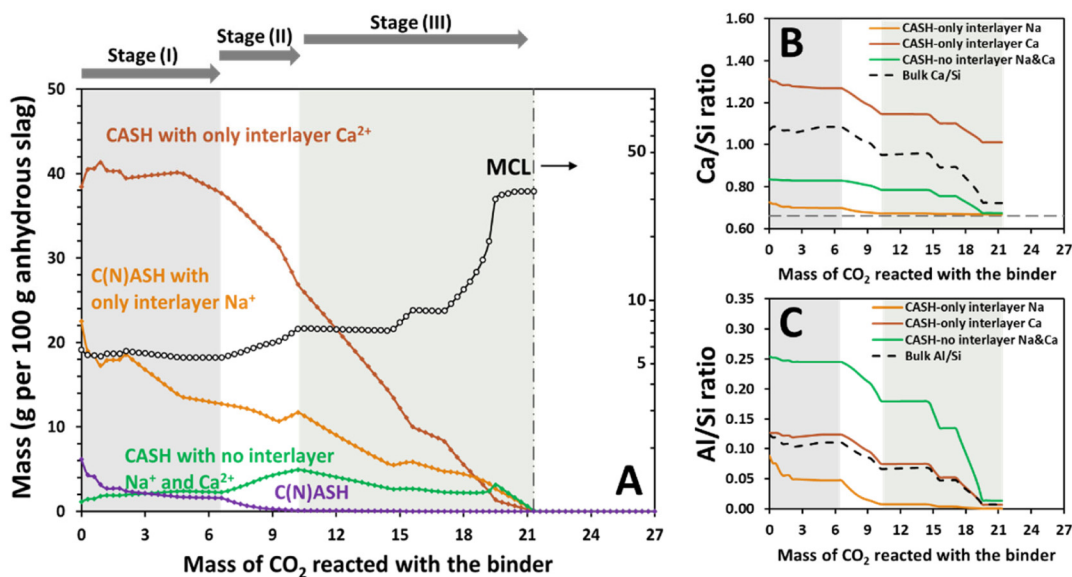
Fig. 8. (A) Mass change of different CNASH_ss end members and mean chain length (MCL) of the CNASH_ss predicted in Na_2CO_3-activated slag paste (4% Na_2O, degree of reaction 70%) predicted under step-wise accelerated carbonation (1% CO_2). The grouping of CNASH_ss end members are explained in Table 1. (B) Changes in the Ca/Si ratio in bulk CNASH_SS and individual C-A-S-H gels with different interlayer species. (C) Changes in the Al/Si ratio in bulk CNASH_SS and individual C-A-S-H gels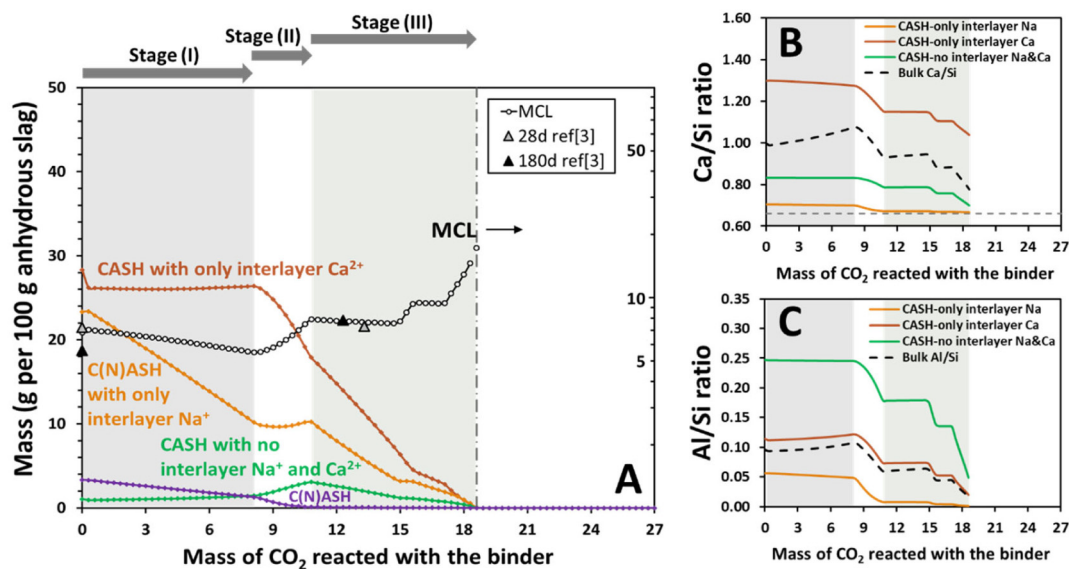 with different interlayer species. The calculation details of MCL from the experimental results shown in [3] are provided in the supporting information.

or years of natural carbonation, where in general a significant decrease in all Q^1 and Q^2 sites was observed, while Q^3 and Q^4 sites increased [4,15,22]. These results suggest an increase in silica chain length, decrease in bulk Ca/Si ratio and loss of tetrahedral Al [48], and the modelling results (Figs. 6 to 8) shown in this study are consistent with such trends. Recently, initial C-(N)-A-S-H gel changes at early stages of carbonation (24 h of atmospheric carbonation exposure) were captured in powdered paste for the NC-AAS system, where the loss of Q^1 and $Q^2(Al)$ sites and the increase of Q^2 sites were observed [3]. The MCL values of the main gel binder before and after carbonation of the two sodium carbonate-activated slag pastes studied in [3] were estimated through the deconvoluted ^{29}Si NMR spectrum (see Table S-2, supporting information). As shown in Fig. 8, the MCL values estimated using experimental data are in good match with the thermodynamic modelling prediction. In addition, it has been observed experimentally that the pore solution pH of partially carbonated AAS concrete is mostly above 10.8 when a mixed activator was used (sodium silicate with sodium hydroxide) [49], similar to the pH of the carbonated pure solution predicted in these binder systems near the exhaustion of the C-(N)-A-S-H gel.
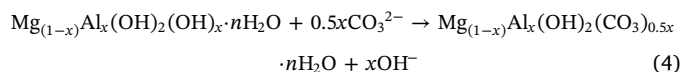
Comparing the phase changes between the different activator systems, prior to carbonation the highest amount of C-(N)-A-S-H gel was predicted to be present in the NS-AAS system while the lowest amount predicted in the NC-AAS system, even though the same degree of reaction of the slag was specified. The total amount of C-(N)-A-S-H gel predicted in NH-AAS was slightly lower than that in NS-AAS. However, the NH-AAS can take up much higher amounts of CO_2 during its stage (I) process in comparison with the other two binder types discussed. Since both the C-(N)-A-S-H gel structure and the pore solution pH do not change signifiantly during the stage (I) carbonation, it appears that under comparable conditions the sodium hydroxide-activated slag cement might be more resilient to carbonation during this carbonation stage in comparison with sodium carbonate and/or sodium silicate-activated slag cement.

However, a different carbonation resistance ranking has been observed experimentally from monolithic samples, where higher carbonation rate was observed for sodium hydroxide-activated slag in comparison with sodium silicate-activated slag [36,45]. In these cases, the lower degree of reaction and much more coarse microstructure developed in the NH-AAS binder before carbonation [12] appears to be dominating the transport of CO_2 within the gel binders, rather than having this controlled mainly by the intrinsic gel chemistry. In comparison, the NC-AAS slag binder can develop denser microstructure than the NH-AAS slag binder under similar activation conditions before carbonation [50]. Therefore, lower carbonation resistance has been observed experimentally in monolithic slag cement samples prepared using sodium carbonate as the activator [3,51,52]. Also, it appears that changes in the aqueous phase pH have a crucial role in the decalcification process of the C-(N)-A-S-H gel. As the modelling results suggest, the pH change in the aqueous phase is predominantly related to the evolution of secondary reaction product phases, which will be discussed in further detail in the next section.

3.1.2. Carbonation of the secondary reaction products

For non-carbonated AAS cements, the main secondary reaction phases formed are hydrotalcite-like phases (Mg,Al-LDH) and AFm phases (Ca,Al-LDH). When AAS is prepared using sodium hydroxide and/or sodium silicate, hydroxylated hydrotalcite was predicted from thermodynamic modelling, consistent with experimental observation [12]. Upon carbonation, the hydroxylated hydrotalcite will be transformed to carbonated hydrotalcite via the exchange of interlayer anions, Eq. (4):

$$Mg_{(1-x)}Al_x(OH)_2(OH)_x \cdot nH_2O + 0.5xCO_3^{2-} \rightarrow Mg_{(1-x)}Al_x(OH)_2(CO_3)_{0.5x}$$

$$\cdot nH_2O + xOH^- \tag{4}$$

The carbonation of hydroxylated hydrotalcite releases OH^- ions into the binder system, increasing the aqueous pH, which slows down the pH drop during carbonation, thus improving the resistance to carbonation. Regardless of the choice of alkali activators, the carbonated hydrotalcite phase is predicted to be thermodynamically stable until the pore solution pH dropped to 12.0, where decomposition of carbonated hydrotalcite and formation of M-S-H gel take place. The predicted pH was maintained at 12.0 until the complete decomposition of carbonated hydrotalcite, corresponding to the predicted initial period of Stage (III) decalcification where the bulk Ca/Si and Al/Si ratio in the C-(N)-A-S-H gel were maintained constant. The decomposition of M-S-H gel was predicted after the pore solution dropped below 8.0, consistent with the experimentally observed stable pH range (around 8–12) for M-S-H gel [53,54].
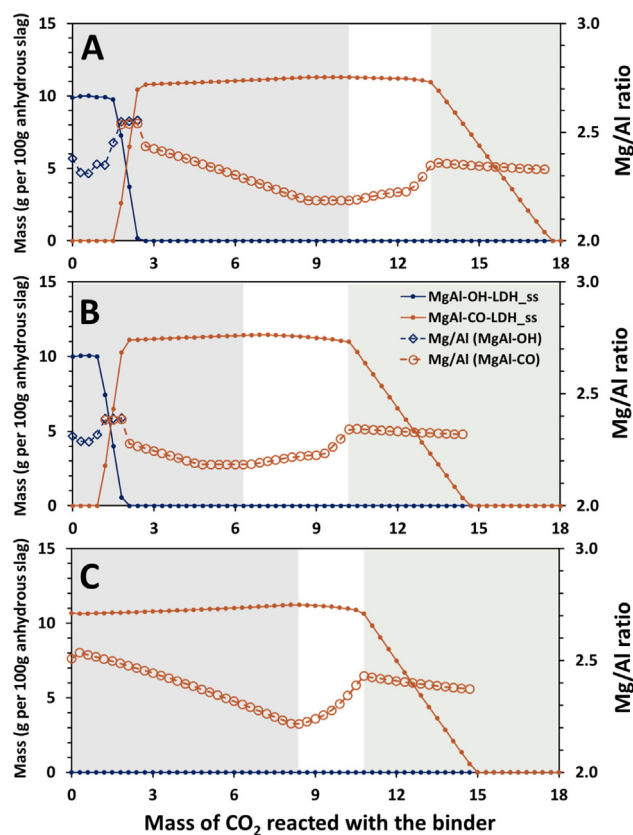
Fig. 9. Mass change of MgAl-OH-LDH_ss and MgAl-CO-LDH_ss, and corresponding bulk Mg/Al ratio of each solid solution, predicted in (A) NaOH-activated slag paste (4% Na$_2$O, degree of slag reaction 70%); (B) Na$_2$O·SiO$_2$-activated slag paste (4% Na$_2$O, Na$_2$O/SiO$_2$ = 1, degree of slag reaction 70%); (C) Na$_2$CO$_3$-activated slag paste (4% Na$_2$O, degree of slag reaction 70%); under step-wise accelerated carbonation (1% CO$_2$). The background shading indicates the carbonation stages proposed in Section 3.1.1.

Fig. 9 shows the mass and elemental ratio changes in the hydroxylated hydrotalcite (MgAl-OH-LDH_ss) and the carbonated hydrotalcite (MgAl-CO-LDH_ss) during the early carbonation. Details regarding the three end members included in hydroxylated hydrotalcite solid solution MgAl-OH-LDH_ss can be found in Table 1 and also in [7,20], and the three carbonated hydrotalcite end members in MgAl-CO-LDH_ss are listed in Table 2. Except for the absence of the hydroxylated hydrotalcite phase in NC-AAS, the changes in mass and elemental ratios predicted in the three AAS types studied are similar. The bulk Mg/Al ratios in both hydrotalcite-like phases were predicted to be between 2.2 and 2.5. As shown in Fig. 9A and B, the Mg/Al ratio in the hydroxylated hydrotalcite phase ranges from 2.3 to 2.5 until full carbonation is reached. In both NH-AAS and NS-AAS, the predicted bulk Mg/Al ratios in the hydroxylated and carbonated hydrotalcite were the same (around 2.4 to 2.5) during the carbonate ion-exchange process. After transformation to carbonated hydrotalcite, its bulk Mg/Al ratio slightly decreased to around 2.2 until the end of initial carbonation, Stage (I). This is likely to be related to the decomposition of monocarbonate during this stage, which releases Al. The bulk Mg/Al ratio then increases during Stage (II) as more Si started to be released from the main binder C-(N)-A-S-H gel, allowing more amorphous aluminosilicate gel to form, and consuming additional Al. During the decomposition of the carbonated hydrotalcite, the predicted bulk Mg/Al ratio is maintained at around 2.3–2.4, likely related to the simultaneous formation of M-S-H gel.

The experimentally observed direct carbonation product of strätlingite, which is the main CaAl-LDH predicted to form in NS-AAS
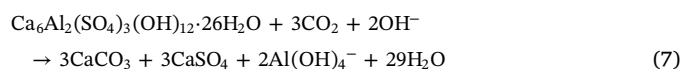
and NH-AAS, was calcite [55]. However, the modelling results shown in Figs. 2 to 4 suggest that in the presence of SO$_4^{2-}$, some monosulfate might also form at the expense of strätlingite during the carbonation process. Since the sulfur contained in blast furnace slag is present primarily in the form of sulfide (S^{2-}) [56], the existence of sulfate species in AAS systems is a result of oxidation of sulfide species in the pore solution, in the presence of oxygen from the air, e.g. Eq. (5):

$$S^{2-} + 2O_2 \rightarrow SO_4^{2-} \tag{5}$$

The oxidation of sulfide is kinetically limited at high pH values [57], as demonstrated in studies where mainly sulfide was observed in cementitious pore solutions even after months and years [58], meaning that in experimental determinations it is possible that significantly less monosulfate will be formed than is predicted by thermodynamic modelling. Significant precipitation of monosulfate has not been observed experimentally from strätlingite exposed to saturated monosulfate aqueous conditions [59]. As carbonation proceeds, monosulfate can react with carbonate ions to form monocarbonate, which eventually carbonates to calcite [60], Eq. (6).

$$3CaO \cdot Al_2O_3 \cdot CaCO_3 \cdot 11H_2O + 3CO_2 + 2OH^-$$
$$\rightarrow 4CaCO_3 + 2Al(OH)_4^- + 8H_2O \tag{6}$$
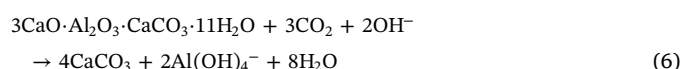
In NC-AAS, formation of monocarbonate was predicted instead of strätlingite, and this gradually carbonates to calcite as the addition of CO$_2$ increases. Monosulfate was not predicted even as a transient phase, likely due to the additional CO$_3^{2-}$ provided by the activator. Carbonated ettringite has been predicted in all alkali-activated slag cements here, as the main sulfate-containing phase after the decomposition of monosulfate. At even greater carbonation extents, ettringite decomposed to calcite, gypsum, and Al(OH)$_4^-$, as suggested by Eq. (7).

$$Ca_6Al_2(SO_4)_3(OH)_{12} \cdot 26H_2O + 3CO_2 + 2OH^-$$
$$\rightarrow 3CaCO_3 + 3CaSO_4 + 2Al(OH)_4^- + 29H_2O \tag{7}$$

For NH-AAS and NS-AAS systems, the direct experimental identification of crystalline strätlingite in non-carbonated samples is rare, but the existence of some form of Ca,Al-LDH (potentially resembling a less-ordered strätlingite) in these alkali-activated slag cements is often suggested by combining SEM-EDX elemental analysis and ^{27}Al MAS NMR spectra [14,15]. The use of siliceous activators might be responsible for the limited crystallisation of strätlingite, and other AFm phases after carbonation, whereas traces of crystalline strätlingite have been identified in NH-AAS binders after 6 months of curing [14]. The decomposition of these AFm phases (mainly strätlingite) can be confirmed by the decrease of octahedrally-coordinated Al in NS-AAS after carbonation, which is observed from ^{27}Al MAS NMR spectra [3,15,22,61]. One significant experimental observation to support this can be found from the sodium silicate activated slag system using a slag with very low MgO content [15], where only Ca,Al-LDH was formed in the original binder, and the octahedral Al site disappeared completely from the ^{27}Al MAS NMR spectra after carbonation.

As for the NC-AAS cements, when early age samples (e.g. 28 days) were exposed to carbonation, the transition from hemicarbonate to monocarbonate could be observed from X-ray diffraction (XRD) analysis [3]. Further carbonation of those samples resulted in decomposition of the monocarbonate phase. However, since the basal reflection peak of monocarbonate is close to that of carbonated hydrotalcite, this phase evolution might not be obvious from XRD characterisation, but a significant reduction in octahedral Al has been observed by ^{27}Al MAS NMR [3].

3.1.3. Formation of aluminosilicate phases

Only a small fraction of natrolite-Na was predicted to form in non-carbonated alkali-activated slag systems, representing the disordered aluminosilicate gel typically identified in sound alkali-activated slag cements [20]. During the carbonation process, the Al(OH)$_4^-$

released from these decomposed secondary phases, together with the Al and Si species released from the decalcified C-(N)-A-S-H gels, can form aluminosilicate gels [3,4,22,45]. Crystallised zeolitic phases are not observed experimentally in most AAS samples either before or after carbonation, likely due to the kinetic limitation of zeolite formation from amorphous aluminosilicate precursors under ambient conditions and at low water content [62]. However, since the thermodynamic properties of well-crystallised zeolite and disordered (glassy) phases with the same chemical compositions appeared to be similar [63,64], aluminosilicate zeolites have been included in this model to represent the amorphous aluminosilicate gel formed during the carbonation process. Despite the different framework structures of the various possible zeolites, their bulk chemical compositions (mainly Si/Al ratios and extra-framework cations) play an important role in determining their Gibbs energy of formation [63]. Therefore, it is reasonable to interpret the different zeolites as representing aluminosilicate gels of different compositions.

The ^{29}Si MAS NMR spectra of carbonated samples often show a broad resonance between -90 and -100 ppm [3,4], likely related to $Q^4(2Al)$ or $Q^4(3Al)$ silica environments, yielding a bulk Si/Al ratio of around 1 to 2 [65]. Among all the zeolite-type phases in the Cemdata18 database [7], natrolite-Na was predicted as the preferred phase. The Ca-rich end member of the natrolite solid solution series, scolecite, has been included in the model here (Na-Ca-NAT_ss), allowing the possible uptake of Ca^{2+} as extra-framework cations to be reflected by the model.

Fig. 10 shows the calculated evolution of the bulk Si/Al, Na/Al and Ca/Al ratios in the zeolite phases (treated collectively) predicted in different alkali-activated slag cements during the carbonation process, corresponding to the results shown in Figs. 2, 3 and 5. Before the full exhaustion of the main C-(N)-A-S-H binding gel, the bulk Si/Al ratio of the aluminosilicate phases remained relatively stable at around 1.4– 1.5, close to that of natrolite-type zeolites. This value is in good agreement with experimental observations in carbonated sodium silicate-activated slag cement, where a bulk Si/Al ratio of 1.4 of the framework tetrahedral aluminosilicate can be calculated from deconvoluted ^{29}Si MAS NMR spectra [4]. Although the bulk Si/Al ratio stayed relatively stable during this carbonation period, the fraction of extra-framework Na^+ decreased and Ca^{2+} increased. This suggests that as the

carbonation proceeds, not all of the Ca^{2+} released from the decomposed C-(N)-A-S-H phase formed calcite; instead, part of the Ca^{2+} might also enter the charge balancing sites of these amorphous aluminosilicate phases. As the decalcification of the main C-(N)-A-S-H binding gel proceeded further, more Si species were released, allowing aluminosilicate phases with higher bulk Si/Al ratios to form. At the final carbonation stage (after the decomposition of M-S-H gel), apart from the Al and Si species dissolved in the carbonated pore solution, almost all of the Si and Al present are in the amorphous aluminosilicate phases. Therefore, NH-AAS and NC-AAS cements showed the same final bulk Si/Al ratio, while NS-AAS showed a higher final Si/Al ratio due to the extra Si provided by the activator.

3.2. The influence of slag chemistry

As discussed in the previous section, the thermodynamic modelling results suggest that in addition to the main reaction product, a C-(N)-A-S-H gel, secondary reaction products (mainly Ca,Al-LDH and Mg,Al-LDH) also play important roles in absorbing CO_2 and controlling the pH changes in the carbonated pore solution, supported by experimental observations [3,15,49]. In this section, the influence of changes in slag MgO and Al_2O_3 contents on carbonation behaviour is discussed (Fig. 11). The bulk elemental ratio in C-(N)-A-S-H gel (CNASH_ss), hydrotalcite (both MgAl-OH-LDH_ss and MgAl-CO-LDH_ss), and aluminosilicate phases predicted in both systems before and after carbonation with different slag compositions are summarised in Table 4.

Fig. 11A and C shows the phase assemblage of NS-AAS and NC-AAS before carbonation, respectively, with varying MgO and Al_2O_3 contents and all other oxide contents unchanged. In both cases, as MgO content increased (and thus Al_2O_3 content decreased), higher amounts of C-(N)-A-S-H gel and Mg,Al-LDH were predicted while the amount of Ca,Al-LDH and aluminosilicate gel decreased, consistent with experimental observations [14–16,66]. The bulk Ca/Si ratio predicted in the C-(N)-A-S-H gel (CNASH_ss) was between 1.0 and 1.2, while the bulk Al/Si ratio slightly decreased as MgO content increased, also in good agreement with experiments [15,16].

The main difffference between the two activated cement systems studied here was in the chemistry of the Mg,Al-LDH phases. In NS-AAS, an Mg/Al ratio of 2.31 was predicted for hydroxylated Mg,Al-LDH produced from slag with high Al_2O_3 but low MgO content, which increased to 3.00 as the Al_2O_3 content decreased. Similar trends have been observed experimentally in analysis of NS-AAS with changing Al_2O_3 and MgO contents [14,67]. In NC-AAS, the initial carbonate provided by the activator was sufficient to carbonate all hydrotalcite within the composition range studied here. In comparison, slightly lower Mg/Al ratios (between 2.23 and 2.95) have been predicted for the carbonated hydrotalcite NC-AAS binder systems with the same bulk Al_2O_3 and MgO contents in the slag.

Fig. 11B and D shows the corresponding phase assemblages during the carbonation process, as snapshots taken when the pore solution pH first dropped to 12.5 in each case. This value has been chosen as indicative for the following two main reasons: i) this is approximately the pH of the colour change boundary indicated by 1% phenolphthalein solution [49]; ii) the oxide film formed on the surface of embedded steel in reinforced concrete is at greater risk of depassivation below pH 12.5 [68,69]. As summarised in Table 4, for both NS-AAS and NC-AAS, the total CO_2 uptake required to reduce the pH to 12.5 was lower at higher MgO content in the slag. Nevertheless, a higher amount of C-(N)-A-S-H gel (CNASH_ss) remained uncarbonated when a slag with higher MgO was used, while less calcite and aluminosilicate phases were predicted. The bulk Ca/Si ratio of the remaining C-(N)-A-S-H gel was slightly higher in NS-AAS than in NC-AAS, while the corresponding predicted Al/Si ratios in these two systems were similar. This is likely due to the formation of less calcite in the NS-AAS system at the same carbonation stage. Comparing the performance of these two systems, when using slag precursors with varing MgO and Al_2O_3 content while maintaining
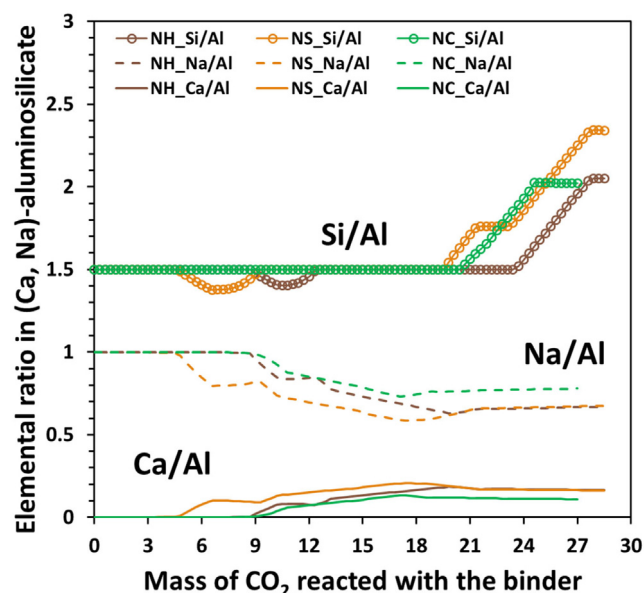

Fig. 10. Evolution of the bulk Si/Al, Na/Al and Ca/Al ratios of the bulk (Ca, Na)-aluminosilicate phases (including all zeolites formed) formed in alkali-activated slag cements produced with different activators, simulated under stepwise accelerated carbonation (1% CO_2) condition. NS, sodium silicate; NH, sodium hydroxide; NC, sodium carbonate.
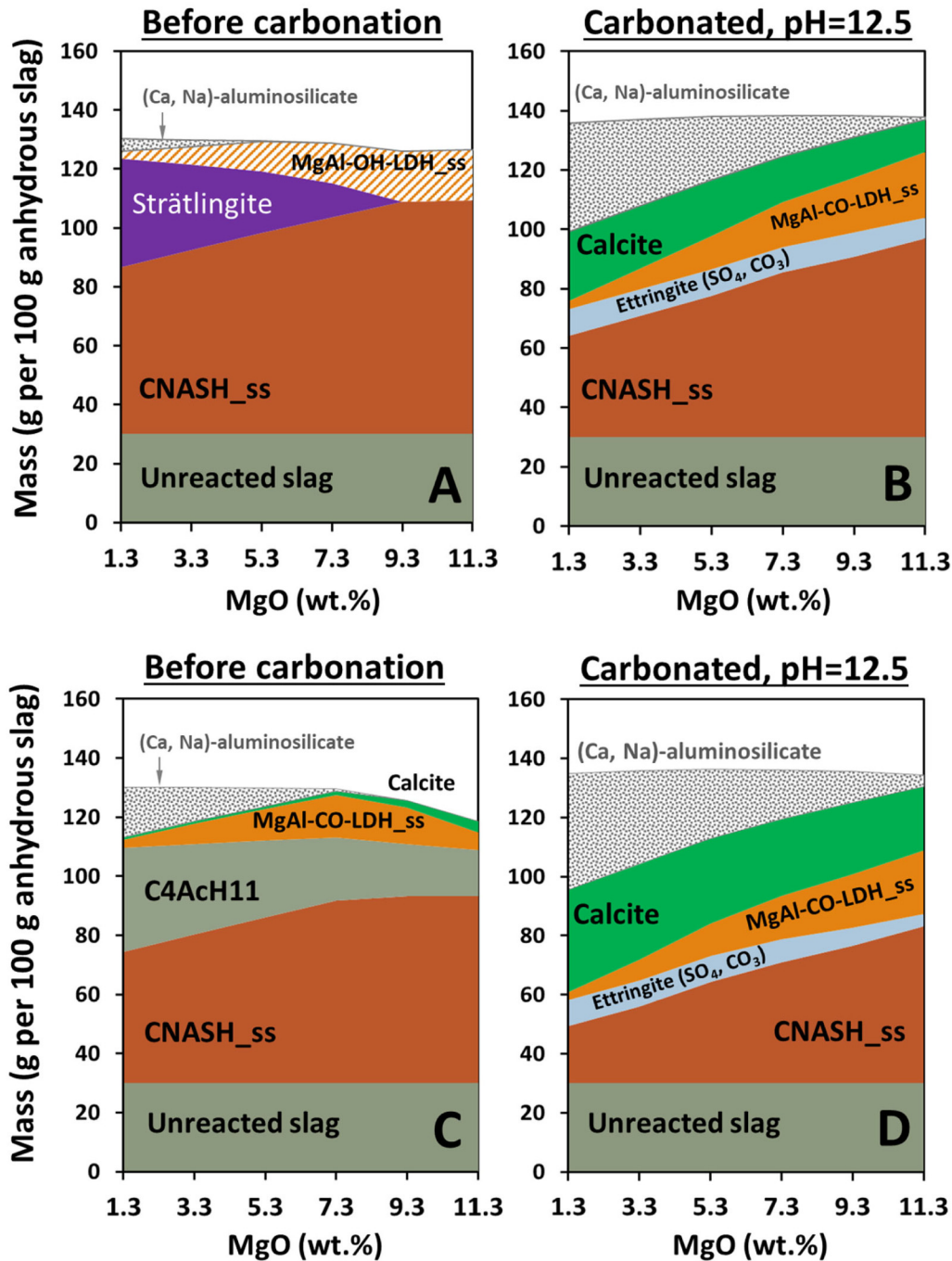
Fig. 11. Phase assemblages of Na_2SiO_3-activated (A & B) and Na_2CO_3-activated (C&D) slag cements with varying content of MgO (1.3 wt% to 11.3 wt%) and Al_2O_3 (17.7 wt% to 7.7 wt%), before and after carbonation. For all simulations, 4% Na_2O and degree of slag reaction 70% are defined. (A) and (C) correspond to simulations before carbonation, and (B) and (D) correspond to simulations after carbonation when the pH first dropped to 12.5. The dotted lines in (B) and (D) show the mass of CO_2 (g) taken up by the binders.

the pH of the carbonated pore solution above 12.5, the maximum amount of CO_2 uptake predicted in the NC-AAS binder system was always about 10–15 wt% higher then that in NS-AAS system.

4. Remarks on model application

Depending on the chemical composition of the slag, and the type and amount of activator used, atmospheric carbonation of alkali-activated slag cements can cause significant changes in the physical and chemical properties of the gel binder, phase assemblages in the solid phase, the pH of the pore solution, and the pore structure of the

cementitious matrix [2,18,45,49]. Thermodynamic modelling of the carbonation process in the AAS systems can adequately simulate the phase evolution in the gel binders during CO_2 exposure, as well as the pore solution pH changes. This information is of great importance to predict the potential stability of the oxide films forming on steel rebars embedded in these cements upon carbonation. The influence of different activators, or slags with different chemical compositions, on the carbonation process can be simulated by the model developed in this study. However, the impact of carbonation on the pore structure cannot be determined from these simulations. Combined with experimental characterisation of the microstructure and carbonation rate, and a

Table 4

Bulk elemental ratios in CNASH_ss, MgAl-OH-LDH_ss, MgAl-CO-LDH_ss and aluminosilicate phases, corresponding to the phase assemblages shown in Fig. 11.

NS-AAS system	CNASH_ss		MgAl-OH-LDH_ss	MgAl-CO-LDH_ss	(Ca, Na)-aluminosilicate	CO_2 uptake (g)
	Ca/Si	Al/Si	Mg/Al	Mg/Al	Si/Al	
Before carbonation						
1.3 wt% MgO[a]	1.08	0.12	2.31	–	1.50	0
3.3 wt% MgO	1.07	0.12	2.31	–	1.50	0
5.3 wt% MgO	1.07	0.12	2.31	–	1.50	0
7.3 wt% MgO	1.12	0.13	2.38	–	–	0
9.3 wt% MgO	1.13	0.12	2.42	–	–	0
11.3 wt% MgO	1.16	0.10	3.00	–	–	0
Carbonated, pH = 12.5						
1.3 wt% MgO	1.02	0.09	–	2.23	1.21	10.2
3.3 wt% MgO	1.01	0.09	–	2.23	1.30	9.6
5.3 wt% MgO	1.01	0.09	–	2.23	1.47	9.0
7.3 wt% MgO	0.97	0.07	–	2.36	1.50	7.8
9.3 wt% MgO	0.91	0.05	–	2.58	1.50	7.2
11.3 wt% MgO	0.88	0.05	–	2.76	1.50	6.3

NC-AAS system	CNASH_ss		MgAl-OH-LDH_ss	MgAl-CO-LDH_ss	(Ca, Na)-aluminosilicate	CO_2 uptake (g)
	Ca/Si	Al/Si	Mg/Al	Mg/Al	Si/Al	
Before carbonation						
1.3 wt% MgO	1.08	0.11	–	2.21	1.50	0
3.3 wt% MgO	1.03	0.10	–	2.37	1.50	0
5.3 wt% MgO	0.99	0.09	–	2.51	1.50	0
7.3 wt% MgO	0.97	0.09	–	2.62	1.50	0
9.3 wt% MgO	0.99	0.09	–	2.95	–	0
11.3 wt% MgO	0.99	0.09	–	2.95	–	0
Carbonated, pH = 12.5						
1.3 wt% MgO	1.02	0.09	–	2.23	1.31	11.7
3.3 wt% MgO	1.01	0.09	–	2.23	1.43	11.1
5.3 wt% MgO	0.97	0.07	–	2.31	1.50	9.9
7.3 wt% MgO	0.92	0.06	–	2.57	1.50	9.0
9.3 wt% MgO	0.86	0.04	–	2.81	1.50	8.4
11.3 wt% MgO	0.84	0.04	–	2.95	1.50	7.5

[a] The corresponding chemical compositions as inputs: 1.3 wt% MgO (17.7 wt% Al_2O_3), 3.3 wt% MgO (15.7 wt% Al_2O_3), 5.3 wt% MgO (13.7 wt% Al_2O_3), 7.3 wt% MgO (11.7 wt% Al_2O_3), 9.3 wt% MgO (9.7 wt% Al_2O_3), 11.3 wt% MgO (7.7 wt% Al_2O_3).

multi-physics transport modelling approach it would be possible to tailor in the future a robust model to fully predict performance of AAS with a specific mix design and exposed under any given carbonation conditions.

The model developed in this study provides novel insight about the chemical processes taking place during the carbonation of alkali activated slag cements. In particular, it clarifies the relationships between the solid phases and pore solutions in carbonated AAS binders. In general, as CO_2 uptake increases in the binder system, the pore solution pH decreases. However, the presence of certain reaction products, such as hydroxylated hydrotalcite, hemi/monocarbonate, and M-S-H gels, can partially buffer the pore solution pH while the CO_2 uptake increases and the carbonation process proceeds. The ability of certain binder systems to take up higher amounts of CO_2 while sustaining a high pore solution pH may significantly improve their overall durability, particularly the resistance to steel reinforcement corrosion due to carbonation, when used in structural applications. In this respect, sodium carbonate-activated slag showed significant evidence of better performance than sodium silicate activated slag cements. The sodium hydroxide-activated slag showed similar performance in sustaining higher pore solution pH at early carbonation stage; however in practice, the coarse microstructure developed in NH-AAS slag cement due to its fast early age reaction kinetics would allow faster ingress of CO_2 into the binder matrix.

For non-carbonated activated slag cements, their mechanical properties, especially compressive strength, are closely related to the density of the microstructure which is mainly contributed by the C-(N)-A-S-H gel. During the carbonation process, the decalcification of C-(N)-A-S-H has been observed to lead to coarsening of the microstructure, resulting in decreased mechanical strength [45,70]. Therefore, it would be preferable to design cementitious systems that can maintain a higher amount of C-(N)-A-S-H gel at the same level of CO_2 uptake, or at the same pore solution pH. In this regard, at the same degree of slag reaction, those containing higher MgO content can give a higher C-(N)-A-S-H gel content and maintain a higher amount of remaining C-(N)-A-S-H gel both at the same mass of CO_2 uptake, and at the same pore solution pH. Together with formation of a higher amount of carbonated hydrotalcite, the denser microstructure favoured by high MgO content in the binders will also slow down the transport of CO_2 within the matrix, contributing to a higher carbonation resistance.

5. Conclusion

The thermodynamic model created in this study can adequately reflect the chemical changes and phase evolution occurring in AAS binders exposed to carbonation. The influence of using different alkali activators and the impact of slag chemistry on the phase evolution of AAS binders during carbonation can be simulated using the proposed model, together with detailed information on the physicochemical changes in the reaction products.

The modelling results show that calcite, carbonated hydrotalcite and aluminosilicate gel with both Na^+ and Ca^{2+} as extra-framework charge balancing cations, are the main carbonation products predicted to form in alkali-activated slag cements before the pore solution dropped below 12.5. At extended degrees of carbonation, carbonated hydrotalcite can decompose to form the transitional phase M-S-H,

which is eventually carbonated to huntite after the pore solution pH dropped below 8.0. The use of different activators mainly affects the phase evolution process and changes in pore solution pH during the carbonation process, while changes in slag MgO and Al_2O_3 contents mainly affect the mass fractions of phases formed and the chemical properties of the secondary reaction products (Ca,Al-LDH and Mg,Al-LDH). The modelling results indicate that sodium carbonate activated slag cements have a better capacity for maintaining higher pore solution pH at the same amount of CO_2 uptake compared with sodium silicate-based cements. When a slag precursor with higher MgO content is used, a higher amount of C-(N)-A-S-H and hydrotalcite are formed, contributing to a denser binder matrix which may show reduced permeability. Theses modelling results are consistent with experimental observations and provide a new tool by which insight into the carbonation of AAS can be generated.

CRediT authorship contribution statement

Xinyuan Ke: Conceptualization, Funding acquisition, Investigation, Methodology, Project administration, Writing - original draft, Writing - review & editing. **Susan A. Bernal:** Funding acquisition, Investigation, Writing - review & editing. **John L. Provis:** Investigation, Writing - review & editing. **Barbara Lothenbach:** Investigation, Writing - review & editing.

Declaration of competing interest

The authors declare that they have no known competing financial interests or personal relationships that could have appeared to influence the work reported in this paper.

Acknowledgements

Appendix A. Supplementary data

Supplementary data to this article can be found online at https://doi.org/10.1016/j.cemconres.2020.106158.

References

[1] H.F.W. Taylor, Cement Chemistry, Thomas Telford, 1997.
[2] S.A. Bernal, X. Ke, M. Criado, S. Mundra, J.L. Provis, Factors controlling carbonation resistance of alkali-activated materials, ACI Special Publication 320 (2016) #36.
[3] X. Ke, M. Criado, J.L. Provis, S.A. Bernal, Slag-based cements that resist damage induced by carbon dioxide, ACS Sustain. Chem. Eng. 6 (2018) 5067–5075.
[4] S.A. Bernal, J.L. Provis, B. Walkley, R. San Nicolas, J.D. Gehman, D.G. Brice, A.R. Kilcullen, P. Duxson, J.S.J. van Deventer, Gel nanostructure in alkali-activated binders based on slag and fly ash, and effects of accelerated carbonation, Cem. Concr. Res. 53 (2013) 127–144.
[5] S.A. Bernal, J.L. Provis, D.G. Brice, A. Kilcullen, P. Duxson, J.S.J. van Deventer, Accelerated carbonation testing of alkali-activated binders significantly underestimates service life: the role of pore solution chemistry, Cem. Concr. Res. 42 (2012) 1317–1326.
[6] R. Pouhet, M. Cyr, Carbonation in the pore solution of metakaolin-based geopolymer, Cem. Concr. Res. 88 (2016) 227–235.
[7] B. Lothenbach, D.A. Kulik, T. Matschei, M. Balonis, L. Baquerizo, B. Dilnesa, G.D. Miron, R.J. Myers, Cemdata18: a chemical thermodynamic database for hydrated Portland cements and alkali-activated materials, Cem. Concr. Res. 115 (2019) 472–506.
[8] R.J. Myers, S.A. Bernal, J.L. Provis, A thermodynamic model for C-(N)-A-S-H gel: CNASH_ss. Derivation and validation, Cem. Concr. Res. 66 (2014) 27–47.
[9] Z. Shi, B. Lothenbach, M.R. Geiker, J. Kaufmann, A. Leemann, S. Ferreiro, J. Skibsted, Experimental studies and thermodynamic modeling of the carbonation of Portland cement, metakaolin and limestone mortars, Cem. Concr. Res. 88 (2016) 60–72.
[10] K. De Weerdt, G. Plusquellec, A. Belda Revert, M.R. Geiker, B. Lothenbach, Effect of carbonation on the pore solution of mortar, Cem. Concr. Res. 118 (2019) 38–56.
[11] A. Fernández-Jiménez, F. Puertas, I. Sobrados, J. Sanz, Structure of calcium silicate hydrates formed in alkaline-activated slag: influence of the type of alkaline activator, J. Am. Ceram. Soc. 86 (2003) 1389–1394.
[12] M. Ben Haha, G. Le Saout, F. Winnefeld, B. Lothenbach, Influence of activator type on hydration kinetics, hydrate assemblage and microstructural development of alkali activated blast-furnace slags, Cem. Concr. Res. 41 (2011) 301–310.
[13] M. Criado, B. Walkley, X. Ke, J.L. Provis, S.A. Bernal, Slag and activator chemistry control the reaction kinetics of sodium metasilicate-activated slag cements, Sustainability 10 (2018) 4709.
[14] M. Ben Haha, B. Lothenbach, G. Le Saout, F. Winnefeld, Influence of slag chemistry on the hydration of alkali-activated blast-furnace slag — part II: effect of Al_2O_3, Cem. Concr. Res. 42 (2012) 74–83.
[15] S.A. Bernal, R. San Nicolas, R.J. Myers, R. Mejía de Gutiérrez, F. Puertas, J.S.J. van Deventer, J.L. Provis, MgO content of slag controls phase evolution and structural changes induced by accelerated carbonation in alkali-activated binders, Cem. Concr. Res. 57 (2014) 33–43.
[16] X. Ke, S.A. Bernal, J.L. Provis, Controlling the reaction kinetics of sodium carbonate-activated slag cements using calcined layered double hydroxides, Cem. Concr. Res. 81 (2016) 24–37.
[17] A. Fernández-Jiménez, F. Puertas, Effect of activator mix on the hydration and strength behaviour of alkali-activated slag cements, Adv. Cem. Res. 15 (2003) 129–136.
[18] N. Li, N. Farzadnia, C. Shi, Microstructural changes in alkali-activated slag mortars induced by accelerated carbonation, Cem. Concr. Res. 100 (2017) 214–226.
[19] H.C. Helgeson, D.H. Kirkham, G.C. Flowers, Theoretical prediction of the thermodynamic behavior of aqueous electrolytes by high pressures and temperatures; IV, calculation of activity coefficients, osmotic coefficients, and apparent molal and standard and relative partial molal properties to 600 °C and 5kb, Am. J. Sci. 281 (1981) 1249–1516.
[20] R.J. Myers, B. Lothenbach, S.A. Bernal, J.L. Provis, Thermodynamic modelling of alkali-activated slag cements, Appl. Geochem. 61 (2015) 233–247.
[21] S.J. Chipera, J.A. Apps, Geochemical stability of natural zeolites, Rev. Mineral. Geochem. 45 (2001) 117–161.
[22] M. Palacios, F. Puertas, Effect of carbonation on alkali-activated slag paste, J. Am. Ceram. Soc. 89 (2006) 3211–3221.
[23] I. Petrovic, A. Navrotsky, Thermochemistry of Na-faujasites with varying Si/Al ratios, Microporous Mater 9 (1997) 1–12.
[24] C.-S. Yang, J.M. Mora-Fonz, C.R.A. Catlow, Modeling the polymerization of aluminosilicate clusters, J. Phys. Chem. C 116 (2012) 22121–22128.
[25] P.S. Neuhoff, Thermodynamic Properties and Parageneses of Rock-forming Zeolites, Ph.D. thesis Stanford University, 1999.
[26] G.K. Johnson, H.E. Flotow, P.A.G. O'Hare, W.S. Wise, Thermodynamic studies of zeolites: natrolite, mesolite and scolecite, Am. Mineral. 68 (1983) 1134–1145.
[27] R.A. Robie, B.S. Hemingway, Thermodynamic properties of minerals and related substances at 298.15 K and 1 bar (10^5 pascals) pressure and at higher temperatures, U.S. Geol. Surv. Bull. 2131 (1995).
[28] T.L. Woods, R.M. Garrels, Thermodynamic Values at Low Temperature for Natural Inorganic Materials: An Uncritical Summary, Oxford University Press, 1987.
[29] E. Königsberger, L.-C. Königsberger, H. Gamsjäger, Low-temperature thermodynamic model for the system $Na_2CO_3 - MgCO_3 - CaCO_3 - H_2O$, Geochim. Cosmochim. Acta 63 (1999) 3105–3119.
[30] S. Miyata, Anion-exchange properties of hydrotalcite-like compounds, Clay Clay Miner. 31 (1983) 305–311.
[31] R.K. Allada, J.D. Pless, T.M. Nenoff, A. Navrotsky, Thermochemistry of hydrotalcite-like phases intercalated with CO_3^{2-}, NO_3^-, Cl^-, I^-, and ReO_4^-, Chem. Mater. 17 (2005) 2455–2459.
[32] R.K. Allada, A. Navrotsky, J. Boerio-Goates, Thermochemistry of hydrotalcite-like phases in the $MgO-Al_2O_3$-CO_2-H_2O system: a determination of enthalpy, entropy, and free energy, Am. Mineral. 90 (2005) 329–335.
[33] G.M. Anderson, D.A. Crerar, Thermodynamics in Geochemistry: The Equilibrium Model, Oxford University Press, 1993.
[34] S.A. Bernal, R. Mejía de Gutiérrez, J.L. Provis, V. Rose, Effect of silicate modulus and metakaolin incorporation on the carbonation of alkali silicate-activated slags, Cem. Concr. Res. 40 (2010) 898–907.
[35] K.-I. Song, J.-K. Song, B.Y. Lee, K.-H. Yang, Carbonation characteristics of alkali-activated blast-furnace slag mortar, Adv. Mater. Sci. Eng. 2014 (2014) 11.
[36] Z. Shi, C. Shi, S. Wan, N. Li, Z. Zhang, Effect of alkali dosage and silicate modulus on carbonation of alkali-activated slag mortars, Cem. Concr. Res. 113 (2018) 55–64.
[37] R.J. Myers, S.A. Bernal, J.D. Gehman, J.S.J. van Deventer, J.L. Provis, The role of Al in cross-linking of alkali-activated slag cements, J. Am. Ceram. Soc. 98 (2014) 996–1004.
[38] S.A. Bernal, R. San Nicolas, J.S.J. van Deventer, J.L. Provis, Alkali-activated slag cements produced with a blended sodium carbonate/silicate activator, Adv. Cem. Res. 28 (2015) 262–273.
[39] X. Ke, S.A. Bernal, O.H. Hussein, J.L. Provis, Chloride binding and mobility in sodium carbonate-activated slag pastes and mortars, Mater. Struct. 50 (2017) 252.
[40] B. Walkley, X. Ke, J.L. Provis, S.A Bernal, Influence of the activator anion on the nanostructure of aged alkali-activated slag cements, Proceedings of the 74th RILEM Annual Week and 40th Cement and Concrete Science Conference, Aug 31 – Sep 04, Sheffield, UK (2020).
[41] J. Schneider, M.A. Cincotto, H. Panepucci, ^{29}Si and ^{27}Al high-resolution NMR characterization of calcium silicate hydrate phases in activated blast-furnace slag pastes, Cem. Concr. Res. 31 (2001) 993–1001.
[42] F. Winnefeld, M. Ben Haha, G. Le Saout, M. Costoya, S.-C. Ko, B. Lothenbach, Influence of slag composition on the hydration of alkali-activated slags, J. Sust. Cem. Based Mater. 4 (2015) 85–100.

[43] K. Jun, S. Norimasa, M. Akira, K. Masao, Precipitation diagram of calcium carbonate polymorphs: its construction and significance, J. Phys. Condens. Matter 21 (2009) 425102.

[44] J.D. Rodriguez-Blanco, S. Shaw, L.G. Benning, The kinetics and mechanisms of amorphous calcium carbonate (ACC) crystallization to calcite, via vaterite, Nanoscale 3 (2011) 265–271.

[45] F. Puertas, M. Palacios, T. Vázquez, Carbonation process of alkali-activated slag mortars, J. Mater. Sci. 41 (2006) 3071–3082.

[46] A.E. Morandeau, C.E. White, Role of magnesium-stabilized amorphous calcium carbonate in mitigating the extent of carbonation in alkali-activated slag, Chem. Mater. 27 (2015) 6625–6634.

[47] M. Criado, X. Ke, J.L. Provis, S.A. Bernal, Structural changes in sodium carbonate activated slag binders induced by CO_2 exposure, 39th Cement and Concrete Science Conference, Bath, 2019.

[48] T.F. Sevelsted, J. Skibsted, Carbonation of C–S–H and C–A–S–H samples studied by ^{13}C, ^{27}Al and ^{29}Si MAS NMR spectroscopy, Cem. Concr. Res. 71 (2015) 56–65.

[49] M.S.H. Khan, A. Castel, Effect of MgO and Na_2SiO_3 on the carbonation resistance of alkali activated slag concrete, Mag. Concr. Res. 70 (2018) 685–692.

[50] A. Fernández-Jiménez, J.G. Palomo, F. Puertas, Alkali-activated slag mortars: mechanical strength behaviour, Cem. Concr. Res. 29 (1999) 1313–1321.

[51] H. Xu, J.L. Provis, J.S.J. van Deventer, P.V. Krivenko, Characterization of aged slag concretes, ACI Mater. J. 105 (2008).

[52] S.A. Bernal, J.L. Provis, R. Mejía de Gutiérrez, J.S.J. van Deventer, Accelerated carbonation testing of alkali-activated slag/metakaolin blended concretes: effect of exposure conditions, Mater. Struct. 48 (2015) 653–669.

[53] D. Nied, K. Enemark-Rasmussen, E. L'Hopital, J. Skibsted, B. Lothenbach, Properties of magnesium silicate hydrates (M-S-H), Cem. Concr. Res. 79 (2016) 323–332.

[54] E. Bernard, A. Dauzères, B. Lothenbach, Magnesium and calcium silicate hydrates, part II: Mg-exchange at the interface "low-pH" cement and magnesium environment studied in a C-S-H and M-S-H model system, Appl. Geochem. 89 (2018) 210–218.

[55] X. Ke, S.A. Bernal, J.L. Provis, Uptake of chloride and carbonate by Mg-Al and Ca-Al layered double hydroxides in simulated pore solutions of alkali-activated slag cement, Cem. Concr. Res. 100 (2017) 1–13.

[56] A. Roy, Sulfur speciation in granulated blast furnace slag: an X-ray absorption spectroscopic investigation, Cem. Concr. Res. 39 (2009) 659–663.

[57] K.Y. Chen, J.C. Morris, Kinetics of oxidation of aqueous sulfide by oxygen, Environ. Sci. Technol. 6 (1972) 529–537.

[58] A. Gruskovnjak, B. Lothenbach, L. Holzer, R. Figi, F. Winnefeld, Hydration of alkali-activated slag: comparison with ordinary Portland cement, Adv. Cem. Res. 18 (2006) 119–128.

[59] M.U. Okoronkwo, F.P. Glasser, Strätlingite: compatibility with sulfate and carbonate cement phases, Mater. Struct. 49 (2016) 3569–3577.

[60] A. Mesbah, C. Cau-dit-Coumes, G. Renaudin, F. Frizon, F. Leroux, Uptake of chloride and carbonate ions by calcium monosulfoaluminate hydrate, Cem. Concr. Res. 42 (2012) 1157–1165.

[61] S.M. Park, J.G. Jang, H.K. Lee, Unlocking the role of MgO in the carbonation of alkali-activated slag cement, Inorg. Chem. Front. 5 (2018) 1661–1670.

[62] C.S. Cundy, P.A. Cox, The hydrothermal synthesis of zeolites: precursors, intermediates and reaction mechanism, Microporous Mesoporous Mater. 82 (2005) 1–78.

[63] J.A. Chermak, J.D. Rimstidt, Estimating the thermodynamic properties (ΔG_f^0 and ΔH_f^0) of silicate minerals at 298 K from the sum of polyhedral contributions, Am. Mineral. 74 (1989) 1023–1031.

[64] A. Navrotsky, Z.-R. Tian, Systematics in the enthalpies of formation of anhydrous aluminosilicate zeolites, glasses, and dense phases, Chem. Eur. J. 7 (2001) 769–774.

[65] G. Engelhardt, D. Michel, High-resolution Solid-state NMR of Silicates and Zeolites, John Wiley & Sons, Chichester, 1987.

[66] X. Ke, S.A. Bernal, J.L. Provis, Layered double hydroxides modify the reaction of sodium silicate-activated slag cements, Green Mater 7 (2019) 52–60.

[67] M. Ben Haha, B. Lothenbach, G. Le Saout, F. Winnefeld, Influence of slag chemistry on the hydration of alkali-activated blast-furnace slag — part I: effect of MgO, Cem. Concr. Res. 41 (2011) 955–963.

[68] K. Tuutti, Corrosion of steel in concrete, KTH, Kungliga Tekniska Högskolan i Stockholm, CBI Forskning 82 (1982) 4.

[69] M. Pourbaix, Thermodynamics and corrosion, Corros. Sci. 30 (1990) 963–988.

[70] S.A. Bernal, R. Mejía de Gutiérrez, J.L. Provis, Engineering and durability properties of concretes based on alkali-activated granulated blast furnace slag/metakaolin blends, Constr. Build. Mater. 33 (2012) 99–108.